PNAS
www.pnas.org

Supplementary Information for

Hydrofoiling Honeybee

Chris Roh, Morteza Gharib

Morteza Gharib
Email: mgharib@caltech.edu

This PDF file includes:

Supplementary text
Figures S1 to S10
Legends for Movies S1 to S5
SI References

Other supplementary materials for this manuscript include the following:

Movies S1 to S5

www.pnas.org/cgi/doi/10.1073/pnas.1908857116

Supplementary Information Text

Materials and Methods

Body and wing kinematics measurement. The honeybees (*Apis mellifera*) were dropped onto a 27.5 cm (w) × 21.3 cm (l) × 5 cm (h) transparent water tank. The depth of the water was maintained at 2.5-5 cm, which is much longer than the width of their wing and wavelength of water wave generated by the bee. The temperature of the water was maintained above 20 °C. The body kinematics of bee's water surface locomotion were recorded at 500-1000 frames·s^{-1} using a high-speed camera (Dantec NanoSense Mk-III; Skovlunde, Denmark). The camera's z-axis was positioned either parallel to the free surface or at a 30° angle. One or two white light sources were placed on the side of the tank or 4 cm above the free surface. The videos showing a bee moving straight across the image plane (or with small deviation) were used for body motion analysis. A total of 12 videos were suitable for body kinematics measurements. The vertical positions of the leading edge were measured for videos with well illuminated wings. A total of 4 videos were suitable for the wing kinematics measurement. Simultaneous measurements of the leading and trailing edge vertical positions were made from videos showing a bee moving orthogonal to the imaging plane of the camera positioned parallel to the water surface.

Honeybee's body velocity was measured using a cross-covariance of their body patterns (SI Appendix, Fig. S2). Using an in-house program written on Matlab (version 2017b; Mathworks Natick MA USA), a pattern on the bee's body from two different time points were cross-correlated to measure the body displacement. The code is available from the corresponding author upon reasonable request. The body position was obtained by integrating the displacements using a trapezoidal method. The velocity was obtained by dividing the displacement by a time step. The acceleration was obtained by differentiating the velocity data with a central difference method. The acceleration data are filtered with a zero-phase lag filter function "filtfilt" in Matlab. The filter design used was 4th order Butterworth filter with cut-off frequency set at four to five times the wing-beat frequency.

Shadowgraph. A collimated white light source was formed by placing a point source at the focal point of a biconvex lens. The light rays travelled through the water and were projected on a light diffuser film placed 1 cm above the water surface. A high-speed camera (Dantec NanoSense Mk-III; Skovlunde, Denmark) was set to face the other side of the diffuser. The wave patterns produced by free-moving bees were recorded at 500 frames·s^{-1}. For the purpose of comparing the wave pattern, the resulting images shown in Fig. 1*B*, and SI Appendix, Fig. S4 are rotated using 'bicubic interpolation' in ImageJ. Unaltered data are shown as movie in Movie S3.

Flow visualisation and particle image velocimetry. For flow visualization, a bee was constrained by guiding it into a fork shaped metal wire (SI Appendix, Fig. S6) fixed to a frame. The width between the two prongs was adjusted to sit between heads and thorax of a honeybee. The bee was constrained from wandering around, but the fork did not touch their wings, and the motion vertical to the water surface were not constrained. 20 µm hollow glass particles (Potters Inc., Malvern, PA, USA) were used to visualize the flow at the surface and in deeper water. The positively buoyant and neutrally buoyant particles were separated by mixing the particles with water and waiting about 4 hour for natural segregation. The buoyant particles at the water surface were skimmed, and the neutrally buoyant particles suspended in the water were siphoned.

To visualize the surface streaming flow, buoyant glass particles were used to ensure that the particles remained at the water surface. An array of light-emitting diodes (Neewer CN-160; Shenzhen, China) were used to illuminate the particles. The flow pattern was recorded with a high-speed camera (IMPERX 210P; Boca Raton, FL, USA) at 100 frames·s^{-1}.

To visualize the deeper water flow, neutrally buoyant particles were seeded. A laser sheet parallel to the water surface illuminated the particles 2.0 mm below the surface. The flowing particle images were recorded with a high-speed camera (Dantec NanoSense Mk-III; Skovlunde, Denmark) at 800 frames·s^{-1}. The flow behind the bee was further measured with a laser sheet illuminating the sagittal plane of the bee. The images were recorded with a high-speed camera (IDT-OS3-S3; Pasadena, CA, USA) at 1000 frames·s^{-1}.

The resulting sequences of particle images were used for pathline visualization and velocity field measurement. The pathlines were visualized by overlaying image sequences using the 'Z Project' function in ImageJ version 1.48 (National Institutes of Health, Bethesda, MD, USA). The velocity fields were obtained using PIVview v.3.5.9 with the following parameters:

(1) 2.0 mm below the free surface: image pair offset, 8; 48×48 pixel windows size; 12 pixel overlap; standard Fast Fourier Transform correlation; multi-grid interrogation with 3 passes; max displacement limit, 5 pixel. Ensemble averaged over 4 second, which is ~260 periods.

(2) Centre Plane: image pair offset, 10; 64×64 pixel windows size; 16 pixel overlap; standard Fast Fourier Transform correlation; multi-pass interrogation; max displacement limit, 10 pixel. Ensemble averaged over 1.5 second, which is ~87 periods.

Mechanical model particle image velocimetry. To measure the flow generated by the mechanical model, a continuous green laser sheet illuminated the mid-section of the wing and the particles underneath. The particle images obtained from the experiment were analyzed using PIVview v.3.5.9 with following parameters: image pair offset, 1; 48×48 pixel windows size; 24 pixel overlap; standard Fast Fourier Transform correlation; single-pass interrogation; max displacement limit, 10 pixel; max displacement difference, 5 pixel; normalized median test threshold, 3.

Detailed Calculations

Detailed Calculations I: Force generated by the wing

The horizontal thrust generated by the wings is calculated using the measured body kinematics (Fig. 2). Assuming minimal interaction between the body and the thruster, the force balance on the bee's body is given as follows, $M \cdot dU/dt = F_{wing} + F_{am} + F_{drag}$, where M is the mass of the bee, U is the body speed, F_{wing} is the force generated by the two wings, F_{am} is the added mass force on the body, and F_{drag} is the form drag on the body.

Both F_{am} and F_{drag} are related to the kinematics of the bee's body. The added mass force is given by the acceleration of the body multiplied by the added mass coefficient, α, $F_{am} = \alpha \cdot dU/dt$. The added mass coefficient is assumed to be constant, which is valid as long as the vertical fluctuation of the body is small. Since the free surface dimple generated by the bee's thorax is approximately hemi-sphere, a half of the added mass coefficient of a sphere is used as an estimate, $\alpha = \rho\pi r^3/3$, where ρ is the water density and r is the radius of the dimple.

At a sufficiently high Reynolds number (*Re*), the form drag scales with velocity squared times drag coefficient, C_D, $F_{drag} = C_D \cdot \rho A U^2/2$, where U is the velocity of the body, A is the frontal area of the wetted body. However, at an intermediate Reynolds number ($1 < Re < 1000$) C_D is a function of *Re* (SI ref. 1). This is because the drag consists of both bluff body drag and skin friction. In such regime, the function for drag coefficient of a sphere is $C_D = 24 \cdot Re^{-1}(1+0.14 \cdot Re^{0.7})$, where $Re = \rho UL/\mu$. Here, L is the diameter of the sphere (L = 2r), and μ is the dynamic viscosity of water. *Re* of the flying honeybees is on the order of 10^4, in which case bluff body drag dominates and C_D is a constant. On the other hand, *Re* of the hydrofoiling honeybees falls under the intermediate regime.

Rearranging the force balance equation and substituting the added mass and form drag relations, the wing generated horizontal force is given as a function of the body velocity and acceleration:

$$\mathrm{F_{wing,x}(t)} = (\mathrm{M} + \alpha) \cdot \frac{\mathrm{dU}}{\mathrm{dt}} + \frac{24\mu}{\rho \mathrm{UL}}\left(1 + 0.14\left(\frac{\rho \mathrm{UL}}{\mu}\right)^{0.7}\right)\frac{\rho \mathrm{AU}^2}{2} \quad (1)$$

The time-averaged thrust generated by the wings can then be calculated by integrating thrust over one period of wing motion and dividing by the period:

$$\overline{F_{wing,x}} = \frac{1}{\mathrm{T}}\int_0^{\mathrm{T}} F_{wing,x}(t)dt \quad (2)$$

The steady-state time averaged acceleration is 0. Therefore,

$$\overline{F_{wing,x}} = \frac{1}{\mathrm{T}}\int_0^{\mathrm{T}}\left(\frac{24\mu}{\rho \mathrm{UL}}\left(1 + 0.14\left(\frac{\rho \mathrm{UL}}{\mu}\right)^{0.7}\right)\frac{\rho \pi \mathrm{L}^2\mathrm{U}^2}{8}\right)dt \quad (3)$$

Using the width of the dimple made by the thorax L ~ 0.01 m (r ~ 0.005 m), $\rho \sim 10^3$ kg/m^3, $\mu \sim 10^{-3}$ kg·m/s and the body speed data given in Fig. 2, the average force generated in one period of wing motion for 60 Hz wing-beat is approximately 20 μN. The time varying forces are shown in SI Appendix, Fig. S3.

Detailed Calculations II: Wave and Flow Momentum Calculation

A control volume around the bee is considered (SI Appendix, Fig. S5). The momentum flux out of the control surface is in the form of surface wave and flow. The horizontal momentum carried by one wavelength of surface wave can be obtained by considering radiation stress, S_{xx}, which is defined as "the excess flow of momentum due to the presence of a wave" (SI ref. 2). For a capillary wave in a deep water (water depth>>wavelength), the expression for radiation stress is

$$S_{xx} = \frac{3}{4}\sigma a^2 k^2 \quad (5)$$

where, σ is the surface tension, a is the wave amplitude, and k is the wave number. The expression is derived for a 2-dimensional wave (equal amplitude and period in a transverse direction). Therefore, the unit of S_{xx} is force per unit width. Multiplying by the width of the wave, W, the average force applied to surrounding fluid in generating one wavelength of surface wave, $\overline{F_{wave}}$, can be expressed as:

$$\overline{F_{wave}} = S_{xx} \times W = \frac{3}{4}\sigma a^2 k^2 W \quad (6)$$

We assume that the momentum carried by surface wave cancels except at the rear due to the bilateral symmetry and fore-aft asymmetry. As a result, we can approximate the momentum carrying wave to have a width, W ~ 0.01m. We further assume that the frequency of the generated surface wave corresponds to the wing-beat frequency. For wing-beat frequency, f = 58 Hz, the wavelength, λ, is 5.3 mm according to the capillary wave dispersion relation, $\omega^2 = \sigma k^3/\rho$, where $\omega = 2\pi f$ and $k = 2\pi/\lambda$. Equation (6) with σ=0.072 N/m, $a=2.5\times10^{-4}$ m, k=1186 m^{-1}, W=0.01 m gives $\overline{F_{wave}}$~50 μN.

The reason for the overestimation is likely due to the 3-dimensionality of the wave field. The diamond shaped wave pattern–resulting from interference of the waves generated by the two wings–indicates that the wave generated behind the bee is not a 2-dimensional wave. The transverse trough and crest would probably reduce the calculated averaged thrust, because the average amplitude of the wave in the transverse direction is smaller. Therefore, the reported value is likely an over-estimation of the force produced by the bee.

The horizontal component of the flow momentum flux out of the control surface, (C_s, SI Appendix, Fig. S5) is approximated as

$$P_{flow} = \rho u^2 A \,, \quad (7)$$

where ρ is the density of water, u is the time-averaged horizontal flow velocity, and A is the jet area. Here, u and A are assumed to be constant; thus, the P_{flow} in equation (7) is equivalent to time-averaged force applied to surrounding fluid in generating flow, i.e., $\overline{F_{flow}}$.

We further assume that only the backward moving central jet contributes to the momentum; u is approximated by half of the maximum horizontal velocity; A is approximated by multiplying the width of central jet at 2 mm below free surface and height of the central jet (SI Appendix, Fig. S7). Substituting the following values, $\rho=10^3$ kg/m^3, u=1.5 cm/s, $A=1\times10^{-4}$ m^2, to the equation (4) gives $\overline{F_{flow}}$~20 μN.

Detailed Calculations III: Dimensional Analysis

Several hydrodynamic forces are involved in the hydrofoiling mechanism. Here, we show that the added mass force (unsteady inertial force) dominates other hydrodynamic forces. Parameters and notations used for describing each force are summarized below. If we assume sinusoidal wing kinematics, then x(t) = A·cos(ωt), $\overline{|\dot{x}|} = (2A\omega)/\pi$, and $\overline{|\ddot{x}|} = (2A\omega^2)/\pi$. It follows that the Ad ~ 20, We ~ 1, Fr ~ 3. These non-dimensional numbers indicate that while steady inertia, surface tension, and gravitational forces are a same order of magnitude, the unsteady inertial force is an order of magnitude larger.

A = amplitude of the wingtip motion = 1 mm

R = Wing span length = 1 cm

W = Wing chord length = 4 mm

f = Frequency = 45 Hz

ω = 2πf = Angular Frequency

T = Period

m_a = Added Mass Coefficient = $\pi\rho R^2/8$

$|(\cdot)| \equiv Absolute\ Value$

$\overline{(\cdot)} \equiv \frac{1}{T}\int_0^T (\cdot)dt$

x = position of a wing tip

$\dot{x} =$ velocity of a wing tip

$\ddot{x} =$ acceleration of a wing tip

$$\text{Unsteady Inertial Force} \sim m_a\overline{|\ddot{x}|} = \frac{\pi}{8}\rho\overline{|\ddot{x}|}R^2(\delta W)$$

$$\text{Steady Inertial Force} \sim \frac{1}{2}\rho\overline{|\dot{x}|}^2R(\delta W)$$

$$\text{Surface Tension Force} \sim \sigma(\delta W)$$

$$\text{Gravitational Force} \sim \rho gAR(\delta W)$$

$$\text{Ad} = \text{Added Mass Number} = \frac{\text{Unsteady Inertial Force}}{\text{Steady Inertial Force}} = \frac{m_a\overline{|\ddot{x}|}}{\frac{1}{2}\rho\overline{|\dot{x}|}^2R} = \frac{\frac{\pi}{8}\rho\overline{|\ddot{x}|}R^2}{\frac{1}{2}\rho\overline{|\dot{x}|}^2R} = \frac{\pi\overline{|\ddot{x}|}R}{4\overline{|\dot{x}|}^2}$$

$$\text{We} = \text{Weber Number} = \frac{\text{Steady Inertial Force}}{\text{Surface Tension Force}} = \frac{\frac{1}{2}\rho\overline{|\dot{x}|}^2R}{\sigma}$$

$$\text{Fr} = \text{Froude Nunber} = \frac{\text{Steady Inertial Force}}{\text{Gravitational Force}} = \frac{\frac{1}{2}\overline{|\dot{x}|}^2}{gA}$$

Detailed Calculations IV: Force calculation from flow under the wing

A control volume method was used to calculate the hydrodynamic force from flow field measured using particle image velocimetry. The control volume under the wing is given in SI Appendix, Fig. S10. The force generated by the wing in the horizontal direction is given by

$$F_{wing,\,x} = \frac{\partial}{\partial t}\int_V \rho u dV + \int_{S1} (\rho u^2 + p\hat{x})dS + \int_{S2} (\rho u^2 + p\hat{x})dS$$

From the time varying flow field (Fig. 5), each term on the right hand side (RHS) can be calculated, except pressure, p. The pressure has steady and oscillatory components. Based on the dimensional analysis, the oscillatory component of $F_{wing,x}$ is dominated by the first term on the RHS. Thus, the main contribution of the pressure to the $F_{wing,x}$ is by the steady time-averaged pressure. This component can be calculated by balancing the vertical momentum,

$$\bar{p}(x) - p_o = -\rho\overline{w^2} + \frac{\partial}{\partial x}\int_{-z}^{0} \rho\overline{u}\overline{w} dz + \rho g\eta$$

Here, we assumed that the height difference of the free surface is small (i.e., ρgη~0). With this assumption, the time-averaged pressure is also calculated based on the flow field measurement.

The resulting $F_{wing,x}$ is then equated to the body kinematic equation from SI Appendix, Detailed Calculations I, from which the body trajectory can be estimated. To find a steady state solution, a time-averaged velocity is guessed and the calculation was iterated until the solution converges. The resulting body position, velocity, and acceleration is plotted in SI Appendix, Fig. S8*E-G*.

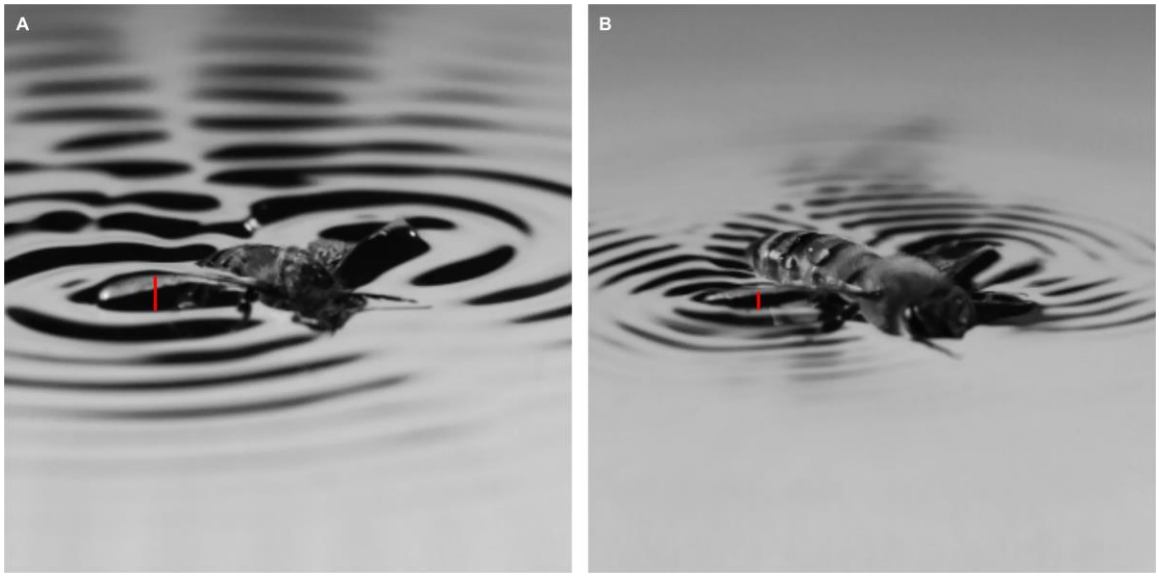

Fig. S1. Wave pattern generated by two different wing-beat frequency. (*A*) Wing-beat frequency 60 Hz. (*B*) Wing-beat frequency 240 Hz. Relative amplitude of the honeybee's wing-beat are shown with red lines.

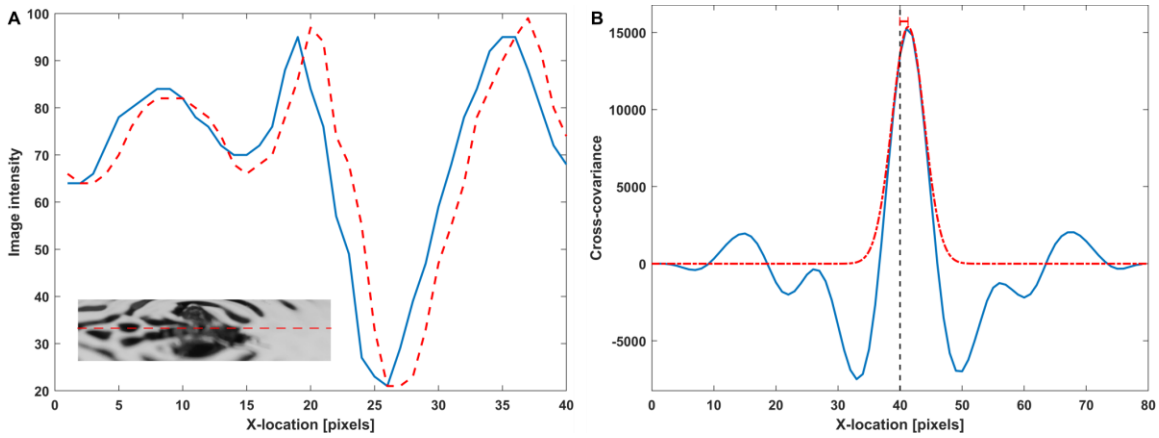

Fig. S2. Cross-covariance body speed measurement. (*A*) A pattern on the bee's body at two different times. The pattern was obtained from the image intensity along the red line shown in the left bottom corner. (*B*) Cross-covariance of the two pattern. The blue line is the cross-covariance result. The red dotted line represent 3-point Gaussian fit. The shift in the peak from the center (marked with black dotted line) represent the displacement of the bee's body.

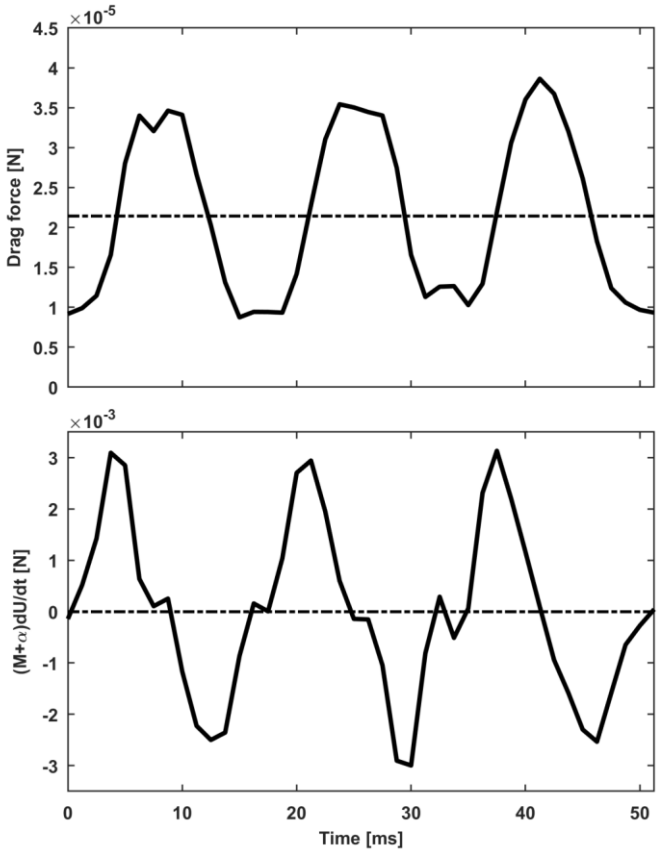

Fig. S3. Force on the bee's body. Top figure shows the form drag on the body. Dotted line represent time-averaged value, 21 μN. Bottom figure shows force needed to accelerate body and added water mass around the body. Dotted line represent time-averaged value, -2.6 μN.

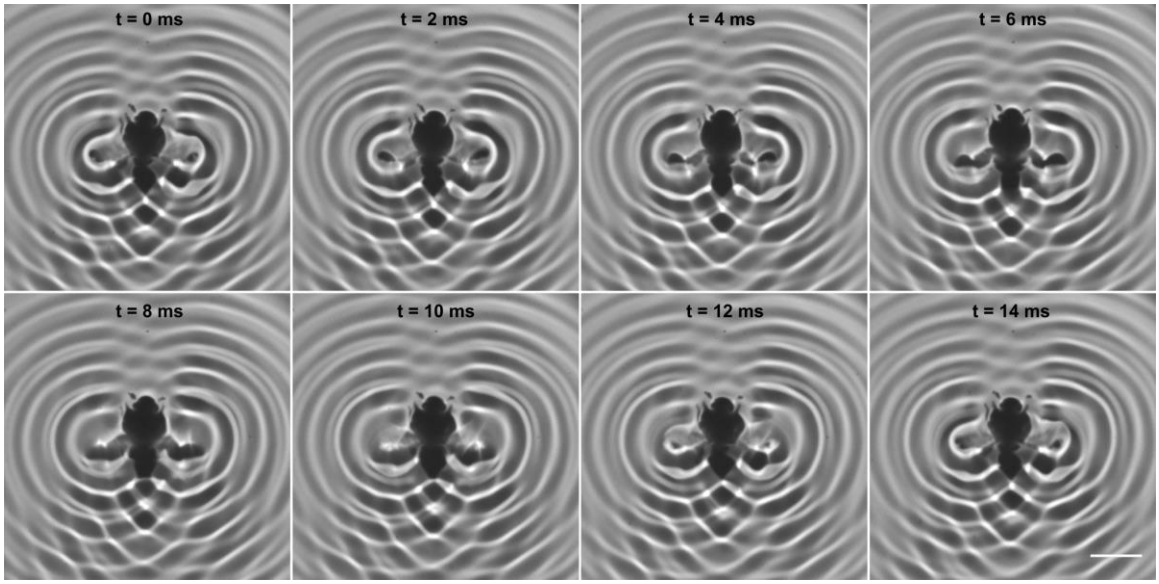

Fig. S4. A full sequence of wave fields generated by a bee. Extracted from shadowgraph video taken at 500 frames·s^{-1} (see Movie S3). The light and dark fringes indicate the wave crests and troughs, respectively. Wing-beat frequency, 69 Hz. Scale bar, 1 cm.

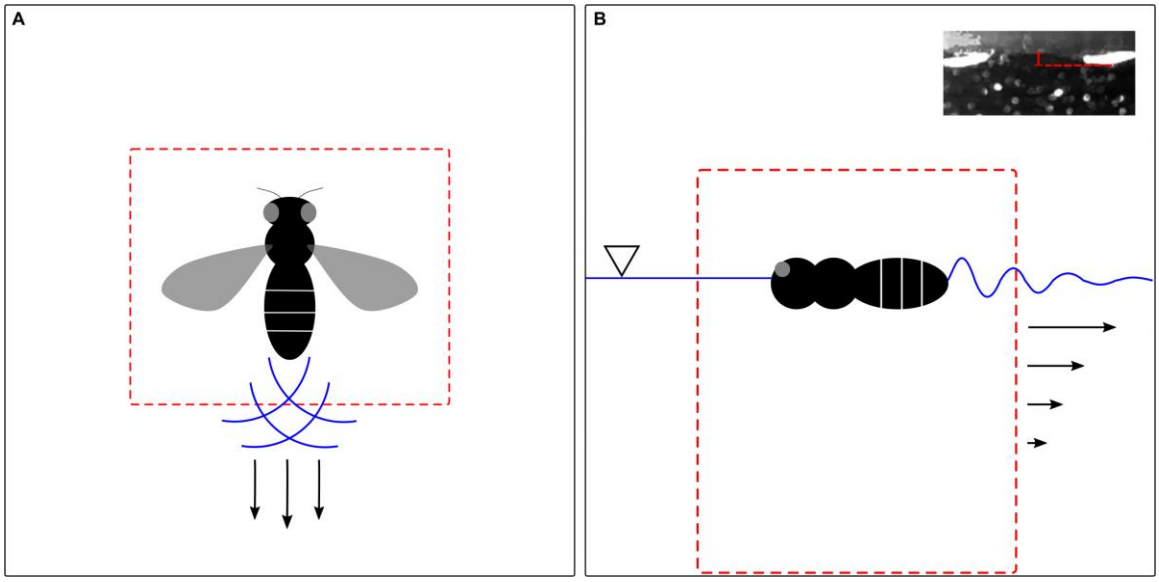

Fig. S5. Control volumes. (*A*) Control volume viewed from the top. (*B*) Control volume viewed from the side. The top right corner shows the amplitude of the wave (~0.5 mm) generated behind the bee's abdomen along its sagittal plane.

Fig. S6. Motion constrainer. A thin metal wire was bent into a fork shape to constrain a honeybee from wandering around. The constrainer did not interfere with the wing motion, and it did not constrain the body motion vertical to the water surface.

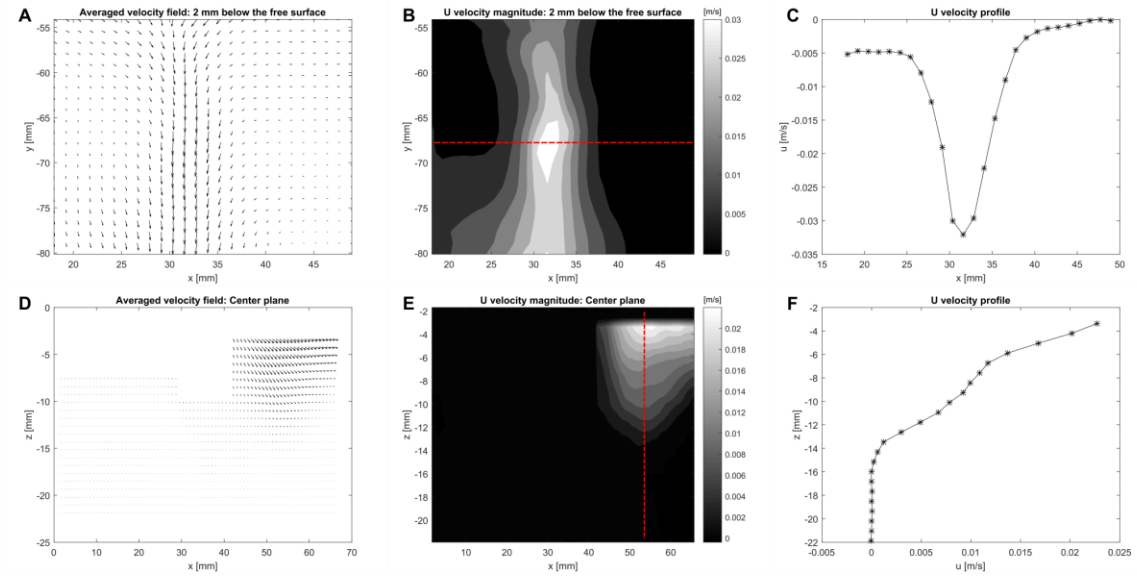

Fig. S7. Particle image velocimetry of flow generated by a bee. (*A*-*C*) Velocity measurement 2 mm below the water surface. (*A*) Velocity field. (*B*) Horizontal velocity magnitude contour plot. (*C*) Velocity profile along the red dotted line in (*B*). (*D*-*F*) Velocity measured at the center plane (sagittal plane). (*D*) Velocity field. (*E*) Horizontal velocity magnitude contour plot. (*F*) Velocity profile along the red dotted line in (*E*).

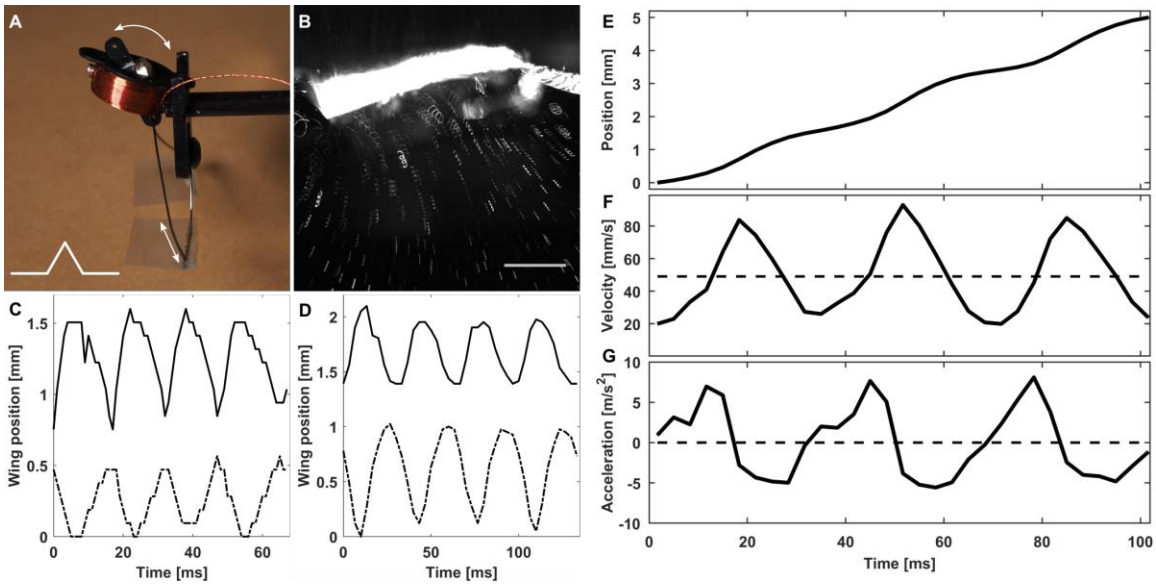

Fig. S8. Mechanical model. (*A*) Mechanical model. The white arrows represent the motion of the device when activated. The lever moves in circular motion, which pulls on the edges of the wing-frame via silk strings. The wing-frame is drawn on the bottom left corner. (*B*) Pathline of the flow generated by the mimicked wing motion. Scale bar = 10 mm. (*C*) Wing kinematics of the bee. The solid and dotted lines represent the vertical motion of the leading and trailing edges, respectively. (*D*) Wing kinematics of the mechanical model. The solid and dotted lines represent the vertical motion of the leading and trailing portions of the wing, respectively. Note the similarity between (*C*) and (*D*). Wing-beat frequency 30 Hz. (*E*-*G*) Position, speed and acceleration calculated from velocity field data in Fig. 5. Dashed line in (*F*) indicates the time averaged speed (49 mm·s^{-1}). Dashed line in (*G*) indicates the time-averaged acceleration (-0.000 m·s^{-2}). Note the similarity with Fig. 2 in the main text.

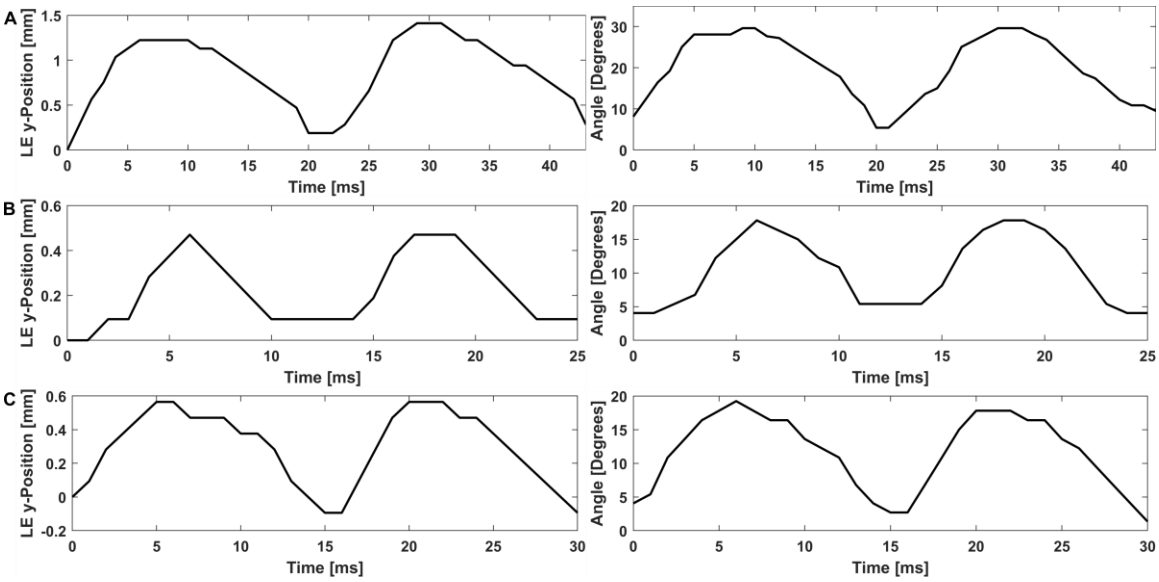

Fig. S9. Honeybee wing kinematics; leading edge position and supination and pronation angle. (*A*) Wing-beat frequency 44 Hz. (*B*) Wing-beat frequencies 63 Hz, reproduced from Fig. 4 (*C*) 83 Hz.

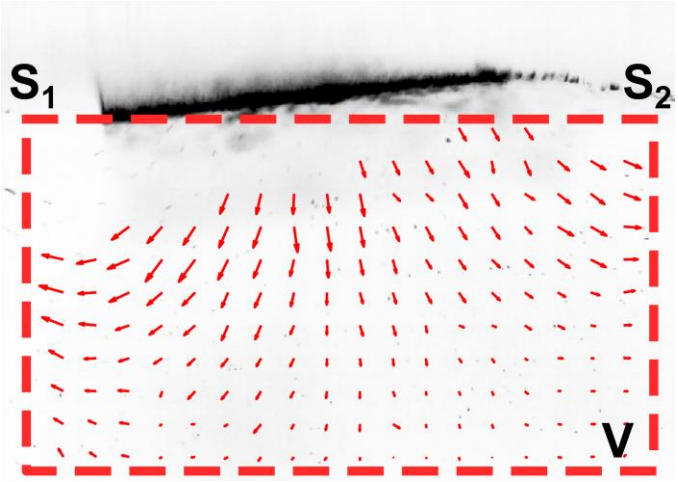

Fig. S10. Control volume under the mechanical wing model. S1, S2, and V corresponds to calculation in SI Appendix, Detailed Calculation IV.

Movie S1 (separate file). Rear view of the honeybee locomotion. Movie is replayed at 1/80 of real time. Still image shown in Fig 1*A*.

Movie S2 (separate file). Front view of the honeybee locomotion. Movie is replayed at 1/80 of real time.

Movie S3 (separate file). Shadowgraph of the honeybee locomotion. Movie is replayed at 1/50 of real time. Still image shown in Fig. 1*B*.

Movie S4 (separate file). Water surface response to the mechanical model wing. Movie is replayed at 1/100 of real time.

Movie S5 (separate file). Flow field under the mechanical model wing. Movie is replayed at 1/30 of real time. Still images are shown in Fig. 5*D*.

References

1. Morrison FA (2013) *An Introduction to Fluid Mechanics* (Cambridge University Press).
2. Longuet-Higgins MS, Stwert RW (1964) Radiation stresses in water waves; a physical discussion, with applications. *Deep-Sea Res* 11:529–562.